Magnetoimpedance spectroscopy of epitaxial multiferroic thin films

Rainer Schmidt,[1,*] Jofre Ventura,[2] Eric Langenberg,[2,3] Norbert M. Nemes,[1] Carmen Munuera,[4] Manuel Varela,[2] Mar Garcia-Hernandez,[4] Carlos Leon,[1] and Jacobo Santamaria[1]

[1]*Universidad Complutense de Madrid, GFMC, Dpto. Física Aplicada III, Facultad de Ciencias Físicas, 28040 Madrid, Spain*

[2]*Universitat de Barcelona, Dpto. Física Aplicada i Óptica, Diagonal Sud, Facultats de Física i Química, Martí i Franquès 1, 08028 Barcelona, Spain*

[3]*Universidad de Zaragoza, Instituto de Nanociencia de Aragón, Mariano Esquillor, 50018 Zaragoza, Spain*

[4]*Instituto de Ciencia de Materiales de Madrid–Consejo Superior de Investigaciones Científicas (ICMM-CSIC), Sor Juana Inés de la Cruz 3, 28049 Madrid, Spain*

(Received 8 May 2012; published 10 July 2012)

The detection of true magnetocapacitance (MC) as a manifestation of magnetoelectric coupling (MEC) in multiferroic materials is a nontrivial task, because pure magnetoresistance (MR) of an extrinsic Maxwell-Wagner-type dielectric relaxation can lead to changes in capacitance [G. Catalan, Appl. Phys. Lett. **88**, 102902 (2006)]. In order to clarify such difficulties involved with dielectric spectroscopy on multiferroic materials, we have simulated the dielectric permittivity ε' of two dielectric relaxations in terms of a series of one intrinsic film-type and one extrinsic Maxwell-Wagner-type relaxation. Such a series of two relaxations was represented in the frequency- (f-) and temperature- (T-) dependent notations ε' vs f and ε' vs T by a circuit model consisting in a series of two ideal resistor-capacitor (RC) elements. Such simulations enabled rationalizing experimental f-, T-, and magnetic field- (H-) dependent dielectric spectroscopy data from multiferroic epitaxial thin films of $BiMnO_3$ (BMO) and $BiFeO_3$ (BFO) grown on Nb-doped $SrTiO_3$. Concomitantly, the deconvolution of intrinsic film and extrinsic Maxwell-Wagner relaxations in BMO and BFO films was achieved by fitting f-dependent dielectric data to an adequate equivalent circuit model. Analysis of the H-dependent data in the form of determining the H-dependent values of the equivalent circuit resistors and capacitors then yielded the deconvoluted MC and MR values for the separated intrinsic dielectric relaxations in BMO and BFO thin films. Substantial intrinsic MR effects up to 65% in BMO films below the magnetic transition ($T_C \approx 100$ K) and perceptible intrinsic MEC up to -1.5% near T_C were identified unambiguously.

DOI: 10.1103/PhysRevB.86.035113 PACS number(s): 73.63.−b, 73.40.−c, 77.22.−d, 85.50.−n

I. INTRODUCTION

Multiferroic materials have attracted major interest in recent years due to potential application in information technology.[1–6] A main aspiration is to design charge storage devices, where information could be written electrically onto a data bit and retrieved magnetically. For such challenges new multiferroic materials are required in thin-film form, where the magnetic properties can be modified by electric fields and vice versa. A large variety of different single-phase compounds[7–11] and different types of heterostructures[12–16] have been considered to obtain such novel multifunctional properties, but large magnetoelectric coupling (MEC) effects of ferromagnetic and ferroelectric order parameters at room temperature, as desired for application, have not been demonstrated convincingly yet. The most prominent example of well-established MEC at elevated temperature may be $BiFeO_3$ (BFO),[9,17,18] where the ferroelectric and antiferromagnetic order parameters are coupled.[19] To introduce the missing ferromagnetic moment into the BFO system, several magnetic cations have been considered as a potential dopant.[7,20] One of the most intensely investigated candidates may be Mn,[21–23] since the parent compound $BiMnO_3$ (BMO) is ferromagnetic below $T_C \approx 100$ K and shows strong indication for ferroelectric order.[24] Therefore, the study presented here was devoted to thin films of these two prominent examples of multiferroic oxides BFO and BMO.

One major problem in the emerging field of multiferroics is the reliable detection of MEC effects. Whereas advanced techniques such as transmittance optical spectroscopy,[25] x-ray absorption[26] or scattering[27] and magnetic field-dependent piezoresponse force microscopy (PFM)[28] are expected to yield unambiguous results, much discussion has arisen over the more frequently used technique of dielectric spectroscopy, which, in multiferroics research, is often combined with applied magnetic fields. A short introduction into the basic principles of dielectric spectroscopy is given in the supplementary material part I.[29]

MEC effects have been reported in a large range of materials by using dielectric spectroscopy,[30–39] where MEC effects were postulated in case that one of the following two criteria was fulfilled:

Criterion A: A change or an anomaly in the temperature dependence of the real part of the dielectric permittivity ε' is measured by varying the temperature across a magnetic transition.

Criterion B: A change in ε' is observed as a result of applied magnetic fields.

There are conclusive reports in the literature though, which demonstrate unambiguously that neither criterion (A) nor (B) is sufficient to safely conclude on an intrinsic MEC effect to occur.[40]

II. SIMULATION OF TWO SERIES DIELECTRIC RELAXATIONS

In order to clarify such difficulties involved with the detection of true intrinsic MEC by dielectric spectroscopy,

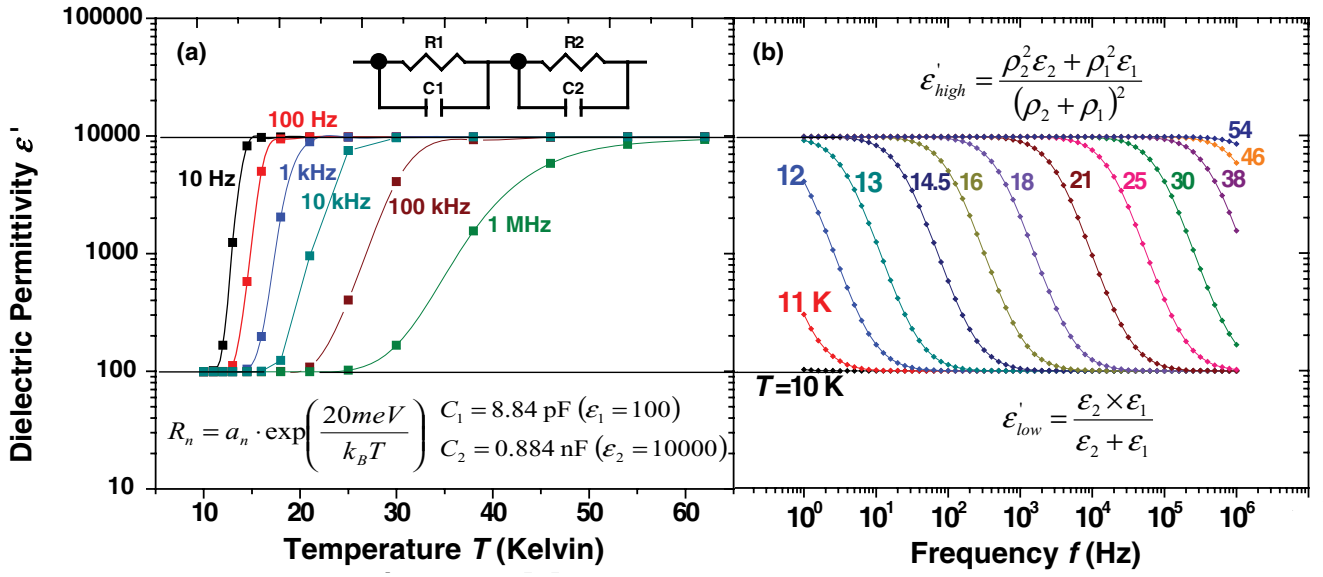

FIG. 1. (Color online) (a) Simulated ε' vs T data for a series of two RC elements (see inset). The ε' vs T curves were calculated at selected frequencies (as indicated) from the analytical expression for $\varepsilon'(f,R_1,R_2,C_1,C_2)$ for a series of two RC elements, where the resistance ($R_n = R_1, R_2$) and capacitance (C_1, C_2) values were substituted into $\varepsilon'(f,R_1,R_2,C_1,C_2)$ according to the expressions shown in the figure inset. (b) Simulated ε' vs f data. The ε' vs f curves were calculated at selected temperatures (as indicated) from the analytical expression for $\varepsilon'(f,R_1,R_2,C_1,C_2)$ for a series of two RC elements. The exact values of the high and low ε' plateaus ($\varepsilon'_{\text{high}}$ and $\varepsilon'_{\text{low}}$) are given, which are equivalent here in both notations: ε' vs T and ε' vs f.

simulations of the dielectric permittivity ε' for a series of two dielectric relaxations have been carried out. In thin films two such series relaxations typically represent one intrinsic film and one extrinsic Maxwell-Wagner-type dielectric relaxation, which can be modeled by a series circuit of two ideal resistor-capacitor (RC) elements. One such ideal RC element is well established to describe the impedance of an ideal intrinsic dielectric relaxation.[41] This RC element model works particularly well for insulators, where the capacitor describes the ability of the material to store charge and the parallel resistor describes the leakage current due to some untrapped charge carriers, bypassing the ideal charge storage element. However, in insulating oxide thin films, the interface between film and electrode often emerges as an additional Maxwell-Wagner-type interface relaxation, and the macroscopic impedance is then well represented by a series of two RC elements. An electrode interface relaxation usually arises from the formation of an interface Schottky-type barrier, which, in turn, is usually a result of the large difference in the electron work functions between the electrode metal and the insulating film oxide.

Impedance spectroscopy allows deconvolution and separate analysis of multiple dielectric relaxations in series, where the data are usually represented on plots of the imaginary vs the real part of the impedance ($-Z''$ vs Z'): for each series dielectric relaxation, usually one semicircle appears in agreement with the RC element model. In multiferroics research, however, dielectric data are often represented in terms of dielectric permittivity ε' vs frequency (f) or ε' vs temperature (T) to directly display changes of ε' as a result of applied magnetic fields (H) or ε' changes with T across a magnetic transition. Figures 1(a) and 1(b) demonstrate the behavior of a series circuit of two model RC elements [see Fig. 1(a) inset] in the notation of ε' vs T [Fig. 1(a)] and ε' vs f [Fig. 1(b)], where R1-C1 represents the intrinsic film contribution and R2-C2 the extrinsic Maxwell-Wagner interface relaxation. For such f- and T-dependent simulations, the values for the model resistors and capacitors were chosen as indicated in the inset of Fig. 1(a). T-independent capacitors C1 and C2 and exponential T dependences for the resistors R1 and R2 were used. The T dependence of the resistors was simulated following an activated Arrhenius-type behavior, since this is commonly observed in insulating oxides. Both resistors were assumed to have the same activation energy (20 meV), whereas the pre-exponential terms a_n [see inset Fig. 1(a)] were chosen differently ($a_2 \gg a_1$) such that R2≫R1: $a_1 = 1\ \Omega$, $a_2 = 100\ \Omega$.

The ε' vs T curves [Fig. 1(a)] were calculated from the analytical expression $\varepsilon'(f,R_1,R_2,C_1,C_2)$ for a series of two ideal RC elements for several selected frequencies. The T-dependent resistance ($R_n = R_1, R_2$) and T-independent capacitance (C_1, C_2) values were substituted into $\varepsilon'(f,R_1,R_2,C_1,C_2)$ for such purpose. The ε' vs f curves [Fig. 1(b)] were simply calculated from the expression $\varepsilon'(f,R_1,R_2,C_1,C_2)$ using fixed resistance and capacitance values at each selected temperature. For the sake of clarity, the nomenclature of ε' is used for the dielectric permittivity as obtained from simulations and experiments at various f and T, whereas ε_2 and ε_1 values represent the extrinsic and intrinsic dielectric permittivity as a representation of the capacitors C2 and C1, respectively, either from simulations or from equivalent circuit fits to the experimental data. ρ_2 and ρ_1 values represent the extrinsic and intrinsic resistivity as a representation of the resistors R2 and R1, respectively.

Equivalent simulations to rationalize the behavior of the dielectric loss, ε'' vs T and ε'' vs f, and the real part of

the conductivity, σ' vs T and σ' vs f, are given in the supplementary material part I.[29]

A. Temperature-dependent dielectric spectroscopy (Criterion A)

Figure 1(a) clearly demonstrates that a steplike increase of ε' with T is fully consistent with the presence of a second extrinsic Maxwell-Wagner relaxation. The T dependence of resistivity in the intrinsic relaxation (ρ_1 vs T) is sufficient to produce this apparent step increase. It is important to note that an exponential T dependence of the intrinsic resistance R1 has been chosen here, whereas different ρ_1-T dependencies would lead to different features in the ε' vs T curves. Not only steplike features but basically any variation in ε' vs T can be the result of a particular intrinsic ρ_1-T relationship. Therefore, Criterion (A) mentioned above is not sufficient *per se* to conclude on true intrinsic magnetocapacitance (MC) and MEC. For reliable detection of intrinsic MC/MEC, the deconvolution of Maxwell-Wagner and intrinsic relaxations is indispensable, which can be achieved best by representing dielectric data in the frequency-dependent notation ε' vs f. Such deconvolution can hardly be performed in the notation of ε' vs T, because the analytical expression for $\varepsilon'(T)$ requires all R-T relationships to be known. Even if this is the case, the expressions obtained are usually complicated for describing and rationalizing the behavior of ε' vs T curves using an equivalent circuit model based on RC elements. An exception to this problem is of course the trivial case of T independent resistors R1 and R2.

B. Frequency-dependent dielectric spectroscopy (Criterion B)

As mentioned before, the ε' vs f curves in Fig. 1(b) were directly calculated from the analytical expression for $\varepsilon'(f,R_1,R_2,C_1,C_2)$ for a series of two RC elements at several model temperatures with the values of the model resistors and capacitors depicted in the inset of Fig. 1(a). A high-dielectric permittivity plateau ($\varepsilon'_{\text{high}}$) at low f is evident, which represents the extrinsic Maxwell-Wagner relaxation (R2-C2), whereas the low permittivity plateau ($\varepsilon'_{\text{low}}$) at high f represents the intrinsic relaxation (R1-C1). This is obvious, because such plateaus approximately coincide with values of the extrinsic and intrinsic capacitors C2 (ε_2) and C1 (ε_1), respectively. In experimental data this scenario occurs regularly where extrinsic relaxations appear at lower f, which enables their discrimination. The simulations in Fig. 1(b) imply unambiguously that attempts to determine the intrinsic permittivity ε_1 by single fixed f measurements in the presence of an additional extrinsic relaxation may generally be doubtful, especially at elevated T and/or at low f. In fact, at 54 K the intrinsic contribution is not visible at all.

Further serious complications for the detection of intrinsic MC/MEC effects can arise out of the fact that the ε' plateaus shown in Figs. 1(a) and 1(b) do not exactly correspond to the values of the capacitors C1 (ε_1) and C2 (ε_2). In case that C1 and C2 are sufficiently different from each other (approximately two orders of magnitude or more), the ε' plateaus usually represent a good approximation for ε_1 (C1) and ε_2 (C2). In any other case, the exact values for the ε' plateaus [$\varepsilon'_{\text{high}}$ and $\varepsilon'_{\text{low}}$ in Fig. 1(b)] need to be considered. This is particularly important for the high ε' plateau at low f representing the extrinsic Maxwell-Wagner relaxation, where the plateau value $\varepsilon'_{\text{high}}$ depends on both resistors R1 (ρ_1) and R2 (ρ_2). This implies that $\varepsilon'_{\text{high}}$ can vary with changing resistivity, for example, due to an extrinsic magnetoresistance (MR) effect as manifested by variations in R2 (ρ_2). This has been pointed out conclusively before by Catalan,[40] stating that MC at a certain fixed f can simply be caused by an MR effect, and therefore, Criterion (B) mentioned above is not a sufficient evidence for MEC.

To summarize, the simulations carried out here clearly suggest that the display of ε' vs T curves is generally inadequate to detect changes in the intrinsic permittivity ε_1, because distinct features in ε' vs T curves are difficult to be directly deconvoluted and separated into intrinsic or extrinsic changes of ε_1, ε_2, ρ_1, or ρ_2, in particular, if only one ε' vs T curve is considered taken at one single fixed f. Deconvolution of all apparent dielectric relaxations is indispensable, which is achieved best by displaying ε' vs f curves at various fixed T. Only after the identification of the intrinsic dielectric relaxation in the sample is it safe to carry out H- and f-dependent dielectric measurements to detect changes in ρ_1 (R1) and ε_1 (C1) as a manifestation of intrinsic MR and MC.

Therefore, in this study presented here, potential MEC effects in BMO and BFO thin films were investigated by dielectric spectroscopy comprehensively and unambiguously by the use of f-, T-, and H-dependent measurements. Fitting ε' vs f dielectric data taken at a fixed T to an equivalent circuit model based on RC elements allowed deconvolution of intrinsic and extrinsic contributions. A magnetic field H was then applied, and the MC of each equivalent circuit capacitor and the MR of each circuit resistor were determined separately for a range of applied magnetic fields. In this way the true MC and MR of the separated intrinsic relaxations of the BMO and BFO films were determined. Such analysis was then repeated at various T to obtain a comprehensive picture of the intrinsic MC and MR behavior.

C. Nonideal dielectric response

In the above Secs. II. A and B, dielectric relaxations have been regarded to be ideal as represented by ideal RC elements. In contrast, the dielectric relaxations identified in the BMO and BFO films presented in this work were all found to be nonideal. In order to still fit the data to an adequate equivalent circuit model, such nonideality in one specific dielectric relaxation was accounted for by using a constant-phase element (CPE) in parallel or instead of an ideal capacitor in the respective RC element.[42–45] The complex impedance $Z_{\text{CPE}}*$ of a CPE is defined as

$$Z^*_{\text{CPE}} = \frac{1}{C_{\text{CPE}}\,(i\omega)^n}, \tag{1}$$

where C_{CPE} is the CPE-specific capacitance. Such CPE capacitance obtained from the equivalent circuit fits can be converted into a real capacitance given in Farad units using a standard procedure.[46] ω is the angular frequency, and n the critical exponent with typical values of $n = 0.6$–1. $n = 1$ constitutes the ideal case of an ideal capacitor for an ideal dielectric relaxation. In a nonideal R-CPE or R-CPE-C circuit,

decreasing n values indicate a broadening of the respective dielectric relaxation peak as a reflection of the broadening of the distribution of relaxation times τ. In an ideal RC element, τ is given by $\tau = \mathrm{RC} = \rho\varepsilon_0\,\varepsilon$. The exact shape of the distribution of τ is not accessible from impedance spectroscopy data, and the exponent n constitutes a semiempirical parameter to reflect increasing width of the distribution of τ by decreasing n values.

III. EXPERIMENTAL

A. Thin-film deposition and characterization

BFO (100-nm) and BMO (50-nm) thin films were grown on conducting (001)-oriented 0.5% Nb-doped $SrTiO_3$ (Nb-STO) substrates following the procedures reported previously.[47,48] Structure, surface morphology, ferroelectricity, and magnetism of both types of film were characterized by x-ray diffraction (XRD), atomic force microscopy (AFM), room-temperature PFM, and superconducting quantum interference device (SQUID) magnetometry as described in the supplementary material.[29] Pt top electrodes (0.9-mm Ø) were sputter deposited onto the film surfaces to facilitate top-top two-terminal dielectric spectroscopy measurements.

B. Magnetoimpedance measurements

Due to the high (metallic) conductivity of the Nb-STO substrates, the sets of Pt top electrodes on the BMO and BFO film surfaces allowed top-top measurements of the impedance twice across the films in the out-of-plane direction as described and justified previously.[43] A QuadTech impedance analyzer was used for dielectric spectroscopy with an applied ac amplitude of 20 mV operating between 20 Hz–1 MHz. Data were collected in the form of capacitance and conductance using a parallel measurement circuit of the impedance analyzer (Cp, Gp) and were converted into the impedance (Z'-Z'') and dielectric permittivity (ε'-ε'') notations by taking into account the effective current cross section and electrode distance.[42] The current cross section was estimated by the electrode surface area A, whereas the electrode distance was taken as twice the film thickness. The out-of-plane measurement configuration employed here leads to relatively moderate nominal thin-film resistance, which is advantageous for the measurement of insulating materials. Equivalent circuit fitting of the dielectric data was performed by using commercial software employing a linear least-squares fitting routine, where the circuit model was fitted to both the real and imaginary parts of the f-dependent data.

In order to facilitate T- and high-H-dependent dielectric measurements, a special sample holder was custom built (Janis Research Ltd., USA), which can fit into a Quantum Design Physical Properties Measurement System (PPMS) providing variable H (up to 140 kOe) and variable T (1.7–320 K). The custom-built probe was necessary in order to minimize the internal probe capacitance (≈0.2 pF) and maximize the internal probe resistance (≈10 GΩ), which is both detrimental for reliable ac dielectric measurements. The sample tray at the bottom of the probe was equipped with spring-loaded drop-down pins in order to ensure optimal contact between the pins and the Pt electrodes on the film surfaces.

IV. STRUCTURAL, SURFACE MORPHOLOGY, FERROELECTRIC, AND MAGNETIC THIN-FILM PROPERTIES

The XRD patterns of BMO and BFO films revealed the absence of parasitic phases, and AFM images and reciprocal space maps evidenced coherent growth and uniform strain. Room-temperature PFM indicated ferroelectricity in BFO, whereas PFM on BMO films failed due to low film resistance at room temperature. All such characterizations are described in detail in the supplementary material.[29] Furthermore, magnetic characterizations of BMO and BFO films are presented in the supplementary materials, revealing a BMO-saturated ferromagnetic moment of $M_{\mathrm{sat.}} \approx 2.5\ \mu_B$/Mn below the Curie temperature $T_C \approx 100$ K. BFO was identified to be antiferromagnetic with a small ferrimagnetic moment of $M_{\mathrm{sat.}} \approx 0.05\ \mu_B$/Fe recorded at 5 K. The BFO antiferromagnetic Curie temperature was found to be above room temperature.

V. DECONVOLUTION OF DIELECTRIC RELAXATIONS

A. Deconvolution of two dielectric relaxations in BMO thin films

Impedance spectroscopy data from a 50-nm BMO thin film are represented in the ε' vs f notation in Fig. 2(a) and in the ε' vs T notation in Fig. 2(b). In both data representations clear signs of two dielectric relaxation processes were obvious as manifested by the existence of two ε' plateaus, $\varepsilon'_{\mathrm{high}}$ and $\varepsilon'_{\mathrm{low}}$. Such plateaus have been discussed above in Sec. II. to be in accordance with the two series of dielectric relaxations as represented by a series of two RC elements, where the low permittivity plateau $\varepsilon'_{\mathrm{low}}$ represents the intrinsic BMO film permittivity and $\varepsilon'_{\mathrm{high}}$ an extrinsic Maxwell-Wagner-type electrode interface relaxation.[43] $\varepsilon'_{\mathrm{low}}$ was found to be ≈35–40, in a similar range as BMO permittivity values of ≈30 reported before.[34,43,49] The data were fitted to an equivalent circuit of a series of two RC elements [see inset in Figs. 2(a) and 2(b)]. Extrinsic parasitic contributions were accounted for by a series inductor L0 describing the inductance of the measurement wires and a series resistor R0 describing the resistance of the conducting substrate, the electrodes and measurement wires.[43] The nonideality of the intrinsic BMO film relaxation was accounted for by a parallel CPE (CPE1) and for the extrinsic relaxation by the replacement of the ideal capacitor by CPE2. In the data presented, the nonideality of the intrinsic relaxation R1-CPE1-C1 is manifested by two distinct features:

(1) The low permittivity plateau $\varepsilon'_{\mathrm{low}}$ is slightly f dependent; ε' modestly decreases with increasing f [Fig. 2(a)] for the low T curves (20–60 K). For an ideal relaxation ($n = 1$), the corresponding ε' plateau would be expected to be f independent. At high f, ε' is increasingly influenced by the inductance L0 and, therefore, shows a relatively sharp upturn.

(2) The ε' drop from $\varepsilon'_{\mathrm{high}}$ to $\varepsilon'_{\mathrm{low}}$ in ε' vs f [Fig. 2(a)] is not as sharp as expected for an ideal intrinsic relaxation R1-C1 as demonstrated in Fig. 1(b).

The experimental and fitted ε' vs f curves in Fig. 2(a) showed good agreement and were both transposed into the ε' vs T notation depicted in Fig. 2(b). Model and data still show reasonable agreement, although slight deviations are obvious, especially at high T. The inset of Fig. 2(b) shows

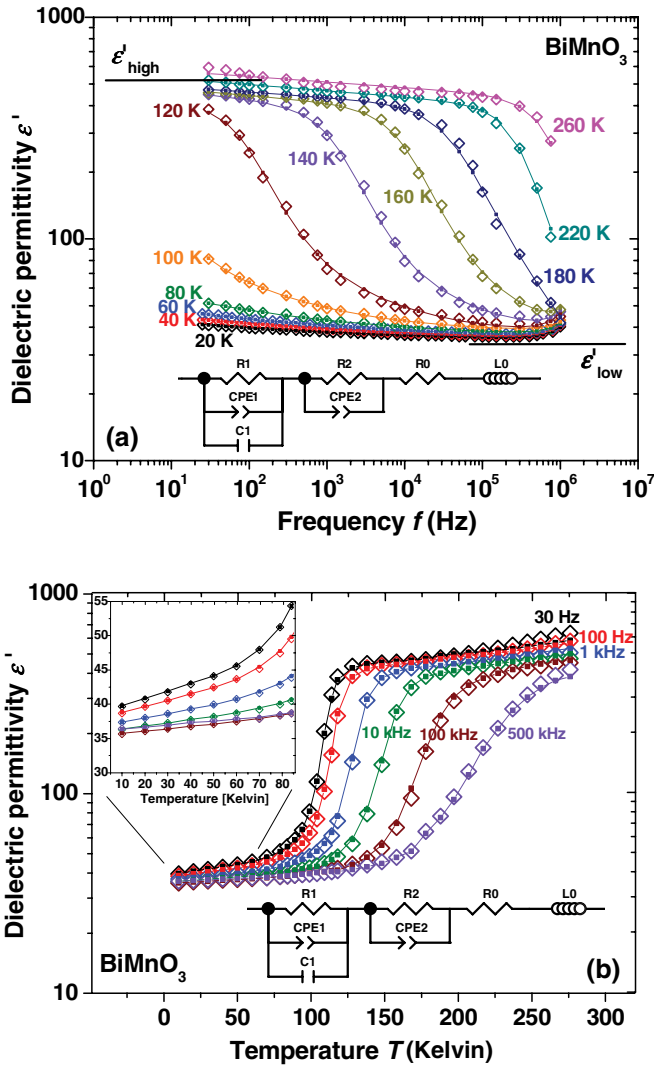

FIG. 2. (Color online) (a) Dielectric permittivity ε' vs f for 50-nm BMO thin film at various selected temperatures as indicated. Open symbols (◇) represent experimental data; full squares (■) and solid lines represent fits to the data using the equivalent circuit depicted below the curves. The occurrence of two ε' plateaus $\varepsilon'_{\text{high}}$ and $\varepsilon'_{\text{low}}$ is consistent with two series dielectric relaxations, represented by a series of two nonideal RC elements, R1-CPE1-C1 and R2-CPE2. R0 and L0 are parasitic contributions. (b) Identical data and fits as in Fig. 2(a), transposed into the ε' vs T notation at selected frequencies as indicated. The inset shows a magnification of the data at low T on identical axes.

a magnification of the data at low T, where a consistent ε' increase with T up to ≈60 K or higher is depicted as expected for a ferroelectric material. Above 60 K the ε' vs T curves start to increase sharply, which is due to the appearance of the second extrinsic Maxwell-Wagner relaxation [see also Fig. 1(a)]. Generally, for the interpretation of dielectric permittivity data, it may always be of vital importance to distinguish between a ferroelectric increase of ε' with T at low temperatures, where the intrinsic relaxation process dominates, and the sharp steplike increase of ε' due to the appearance of a second relaxation at higher T.

The inset of Fig. 2(b) demonstrates clearly the CPE behavior, where the f dependence of ε' especially at lower f is evident. At high f the inductance L0 has an increasing influence, as mentioned above.

B. Detection of one dielectric relaxation in BFO thin films

Impedance spectroscopy data from a ferroelectric 100-nm BFO thin film are shown in Figs. 3(a) and 3(b) in the ε' vs f and ε' vs T notations, respectively. The data showed features of only one dielectric relaxation at the T range investigated, which was associated with the intrinsic film contribution. The equivalent circuit consisted therefore of one nonideal R-CPE element in series with the extrinsic parasitic contributions L0 and R0, as depicted in the inset of Fig. 3(b). It is likely that a second Maxwell-Wagner-type interface relaxation exists but may be visible only at higher T.[43] In fact, some indication

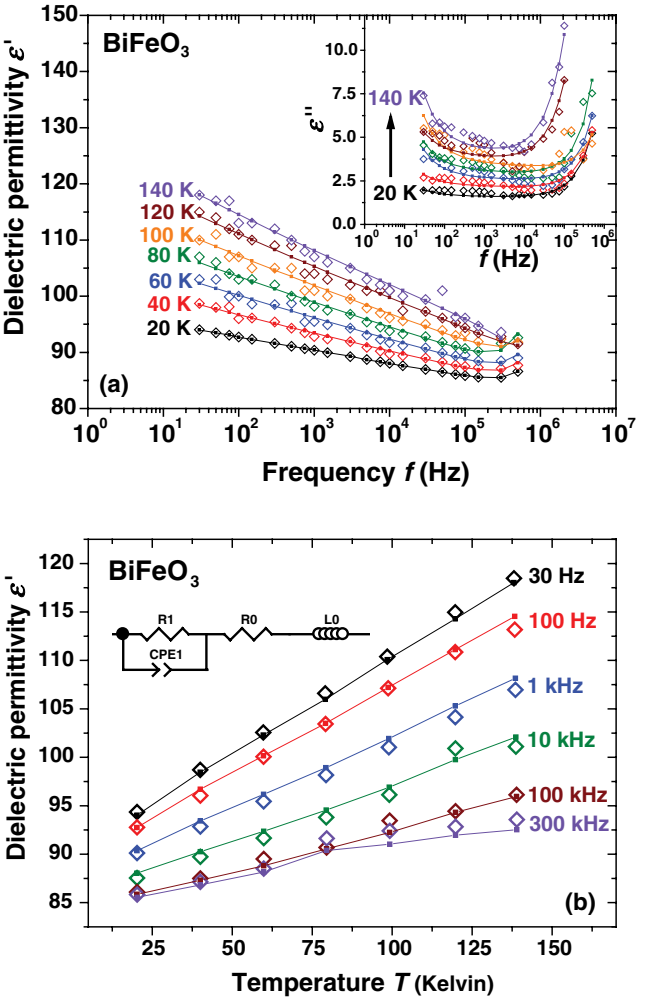

FIG. 3. (Color online) (a) ε' vs f for 100-nm BFO thin film at selected temperatures as indicated. Open symbols (◇) represent experimental data; full squares (■) and solid lines represent fits to the data using the equivalent circuit depicted in the inset of Fig. 3(b). Only one dielectric relaxation is indicated and is represented by one nonideal RC element R1-CPE1. R0 and L0 are parasitic contributions. Inset: Dielectric loss ε'' vs f. An approximately constant loss is indicated at low T. (b) Identical data and fits as in Fig. 3(a), transposed into the ε' vs T notation at selected frequencies as indicated. The equivalent circuit model is depicted above the curves.

for such an additional relaxation was encountered at higher temperatures (data not shown), but for a fully developed second relaxation, the temperature range investigated was too low. Contrarily, the BMO interface relaxation had been detected already at much lower T, which is solely a consequence of the lower intrinsic resistivity ρ_1 of the BMO film. The BFO ε' vs f curves in Fig. 3(a) show considerable f dependence, which is the equivalent trend as for the BMO films [as shown in Figs. 2(a) and 2(b)] associated with CPE-type behavior and a broadening of the distribution of τ. The upturn in ε' at high f is again due to the effect of L0.

Figure 3(a) is plotted on a semi-logarithmic scale and the good linearity of all curves implies that ε' may exhibit an unusual logarithmic f dependence $\varepsilon' \sim -A \ln f$, where the slope A increases approximately linearly with T (on the semilogarithmic scale). As it follows from Kramers-Kronig relationships, the dielectric loss ε'' is found to be approximately f independent [Fig. 3(a) inset], especially at lower T. This "flat-loss" behavior has been previously observed in ferroelectric materials and was ascribed to be a universal feature of ferroelectricity.[50,51] The logarithmic f dependence of the real part of dielectric permittivity ε' implies that electric polarization decays logarithmically in the time domain when an equilibrium polarization is achieved by an electric field, and the latter is suddenly removed. This is reminiscent of the logarithmic time-dependent relaxation for magnetization in ferromagnets, which can be understood in terms of an exceptionally broad distribution of τ associated with domain wall pinning and its relaxation dynamics in the creep regime.[52] Creep phenomena, which are generally related to glassy behavior in disordered systems, are characteristic of domain-wall pinning effects in magnetic materials, and they have been proposed to be generally valid for pinning processes in all ferroic systems: ferromagnetics, ferroelectrics, and ferroelastics.[53,54]

The logarithmic f dependence of ε' may be difficult to be distinguished though from a weak Jonscher-type universal power law of the form $\varepsilon' \sim A/f^{1-n}$ with n close to 1.[55] It has been shown previously that the Jonscher's universal power law is consistent with an R-CPE circuit,[56,57] and indeed good fits are obtained by using the model shown in Fig. 3(b), leading to CPE exponents n close to 1 [Fig. 4(c)]. The T dependence of ε' at fixed f [Fig. 3(b)] confirms the ferroelectric behavior of the BFO thin film.

C. Equivalent circuit-fitting parameters of BMO and BFO films

Using the equivalent circuits shown in the insets of Figs. 2 and 3, the BMO and BFO intrinsic and extrinsic relative dielectric permittivity ε_1 (C1) and ε_2 (C2), resistivity ρ_1 (R1) and ρ_2 (R2), and the CPE exponents n were determined at various T. The resulting T dependences of such deconvoluted parameters are presented in Figs. 4 and 5. The BFO intrinsic film permittivity ε_1 increases uniformly from 100 to 130 with T (Fig. 4). This may be associated with ferroelectricity confirming the trends observed in ε' vs T [Fig. 3(b)]. The intrinsic BMO permittivity $\varepsilon_1 \approx$ 35–45 shows a modest increase up to 75 K, again consistent with ferroelectricity and the trends observed in ε' vs T (inset of Fig. 2(b). At higher T around the magnetic transition $T_C \approx 100$ K, the BMO intrinsic

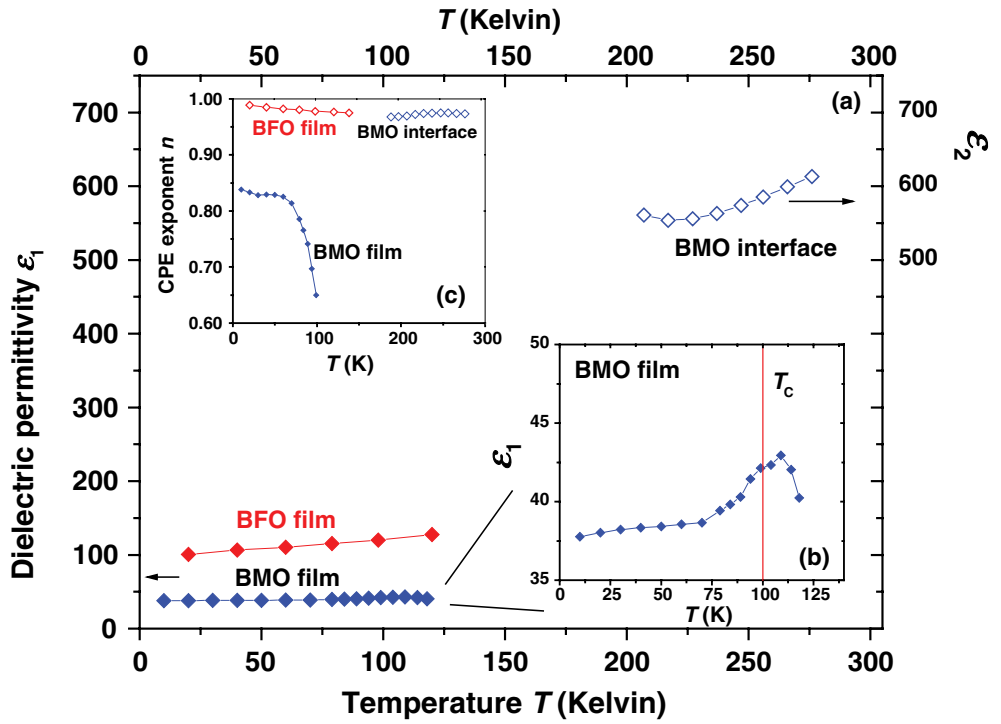

FIG. 4. (Color online) (a) BMO and BFO intrinsic and extrinsic dielectric permittivity ε_1 and ε_2 vs T, obtained from C1/CPE1 and CPE2 in the respective equivalent circuit fits. (b) Magnification of the intrinsic BMO permittivity ε_1 displaying signs of MEC near T_C. (c) CPE exponents n, indicative of more ideal ($n \approx 1$) or less ideal ($n < 1$) character of the respective dielectric relaxation.

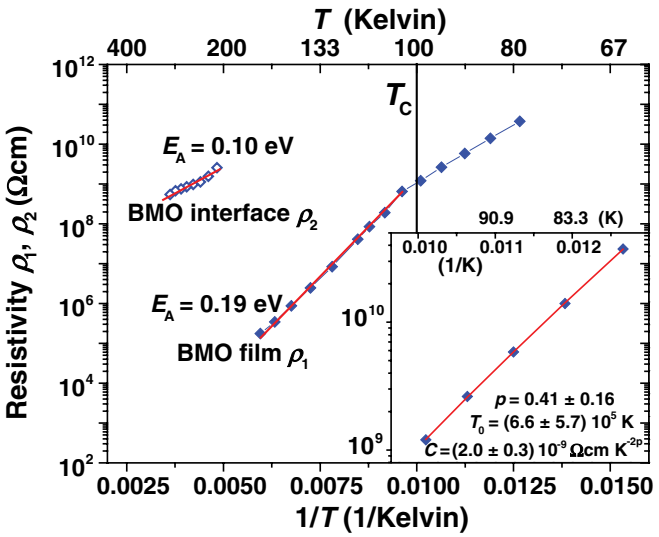

FIG. 5. (Color online) BMO intrinsic and extrinsic resistivity ρ_1 and ρ_2 vs T, obtained from R1 and R2 in the BMO equivalent circuit. ρ_1 shows correlation with T_C. The activation energies E_A are given in electron volts. Solid lines are linear Arrhenius fits. Inset: Magnification of the ρ_1 vs T data below T_C showing signs of VRH. The solid line represents the VRH fit with the fitted parameters given.

ε_1 vs T curve displays a peak structure as demonstrated in the enlarged inset of Fig. 4(b). This may well represent an intrinsic MEC response of ε_1 to the BMO magnetic transition at T_C, since all extrinsic contributions had been deconvoluted and were accounted for by means of the equivalent circuit. The peak in ε_1 vs T is consistent with previous work,[49] where the peak was more strongly pronounced though. Since the peak structure observed here is rather weak, it can hardly be resolved from the experimental data presented in Fig. 2(b) and only emerges from the fits. The extrinsic BMO interface permittivity ε_2 is displayed in Fig. 4(a) showing values of 550–600, which is slightly below the standard for such a type of relaxation.[41] Precise values for the interface permittivity ε_2 are accessible only above 200 K, because below 200 K, the interface resistivity ρ_2 is high and cannot be resolved (see Fig. 5). As demonstrated above in Sec. II. [Fig. 1(b)], the high f plateau $\varepsilon'_{\text{high}}$ contains contributions from the interface resistance R2, and the extrinsic dielectric permittivity ε_2 can, therefore, be determined reliably from the $\varepsilon'_{\text{high}}$ plateau only if this extrinsic resistance R2 can be resolved and determined.

Figure 4(c) shows the CPE exponent n for the various BFO and BMO relaxations. The intrinsic BMO film relaxation shows a strongly increasing nonideality above 75 K, which is manifested by a drop of n with increasing T. This may well be consistent with a broadening of the distribution of τ, possibly as a reflection of the magnetic transition T_C. This, in turn, points toward increasing disorder in the BMO film with increasing T due to the nearby onset of paramagnetism above 75 K.

Figure 5 demonstrates the BMO thin film and interface resistivity ρ_1 and ρ_2 on plots of ρ vs reciprocal T. The intrinsic film BMO charge transport shows correlation with T_C, since the ρ_1 vs $1/T$ curve shows clearly modified T-dependence above and below T_C:

– Above T_C, thermally activated transport is indicated with a T-independent activation energy E_A of 0.19 eV, in excellent agreement with previous work (0.2 eV).[49]

– Below T_C, the thermal activation of charge transport is weaker as reflected by a reduced slope of the ρ_1 vs $1/T$ curve implying a lower activation energy E_A. Careful examination of the ρ_1 vs $1/T$ curve reveals a slight T dependence of E_A as highlighted in the inset of Fig. 5.

This T dependence of the intrinsic BMO activation energy E_A can be described satisfactorily by a variable-range hopping (VRH) power law of the form[58]

$$\rho_1 = CT^{2p} \exp\left(\frac{T_0}{T}\right)^p, \tag{2}$$

where C is a T-independent sample-specific parameter, T_0 a characteristic temperature, and p the critical hopping exponent. Although only few data points are available here to suggest VRH charge transport to occur, possibly between defect Mn^{2+} and Mn^{3+} cations, it should be noted that the T dependence of charge transport in mixed valence manganite-hopping systems commonly follows VRH laws.[59,60] A linear least-squares routine was employed to fit the Arrhenius $\ln(\rho_1)$ vs $1/T$ curve to Eq. (2) for $T \leqslant T_C$. The VRH fit and the fitted parameters are presented in the inset of Fig. 5, where $p = 0.41 \pm 0.16$ in agreement with previous results on perovskite mixed-valence manganite thin films ($p = 0.4$).[61] Generally, the intrinsic BMO film resistivity ρ_1 below T_C is strongly increased here as compared to Ref. 49, which may point toward a better film quality and reduced leakage. The higher resistivity suggests that the Mn cations are predominantly in the nominal Mn^{3+} oxidation state and the potential Mn^{2+} defect valence state may occur in small amounts only in the films presented here.

The intrinsic resistivity ρ_1 of the BFO film was high at all T investigated and could not be resolved. Therefore, the film quality may be regarded satisfactory with minimized leakage. In the equivalent circuit fits, the resistors R2 for the BMO interface and R1 for the film BMO and BFO contributions were always set to infinity in case that the impedance data did not allow resolving high resistance.

VI. MAGNETIC FIELD-DEPENDENT DIELECTRIC CHARACTERIZATIONS

After rationalizing the presence of extrinsic and intrinsic dielectric relaxations in BMO and the single intrinsic relaxation in BFO films, the MR and MC in both types of film were now determined. The f-dependent BMO and BFO film impedance was measured at selected fixed T repeatedly under various fixed applied H. The data was fitted using the equivalent circuits shown in Figs. 2 and 3, and the H dependence of the intrinsic circuit parameters R1, C1 (for BMO), and CPE1 (for BFO) were determined to obtain the intrinsic MR and MC.

The complex impedance notation, $Z^* = Z' + \mathrm{i}\, Z''$, is presented in Fig. 6(a) in terms of $-Z''$ vs Z' curves for the BMO film at 95 K close to T_C, where in such plots a semicircle

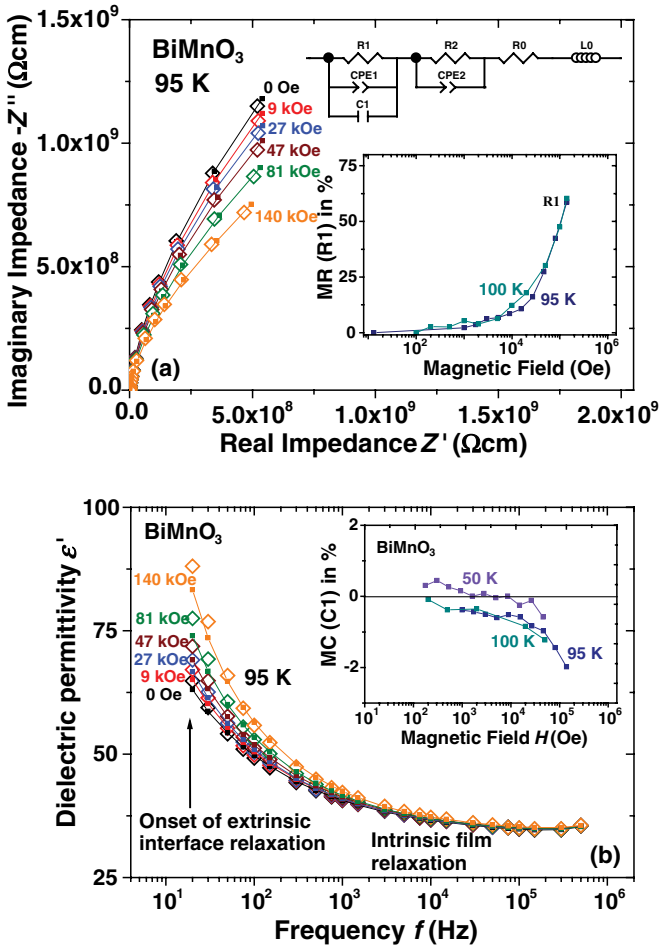

FIG. 6. (Color online) (a) BMO imaginary part of the impedance $-Z''$ vs real part Z' at 95 K for selected applied magnetic fields H (Oersted) as indicated. Open symbols (◇) represent experimental data; full squares (■) and solid lines represent fits to the data using the equivalent circuit depicted at the top of the curves. The decreasing size of the semicircle indicates MR of the intrinsic BMO film relaxation. The inset displays MR (%) vs H (Oersted) at 95 and 100 K, where MR=[R(H=0)–R(H)]/R(0). (b) ε' vs f for 50-nm BMO thin film at 95 K for selected applied magnetic fields H (Oersted) as indicated. Open symbols (◇) represent experimental data; full squares (■), and solid lines represent fits to the data using the equivalent circuit depicted in Fig. 6(a). The inset displays MC (%) vs H (Oersted) at 50, 95, and 100 K, where MC=[C(H=0)–C(H)]/C(0).

is expected for each relaxation and the semicircle diameter corresponds to the resistivity of the respective relaxation.[42] The partial semicircles in Fig. 6(a) are a manifestation of the intrinsic relaxation, whereas the extrinsic interface resistance is large and not accessible at this T and f range. Although the intrinsic film semicircle is not fully displayed, the diameter may be extrapolated readily. On increasing H, the semicircle diameter decreases, which entails that ρ_1 decreases as a result of MR. The H-dependent R1 values allowed calculating the intrinsic MR defined by MR=[R(H=0)–R(H)]/R(0). The inset of Fig. 6(a) shows rather high MR of up to 65% at 95 and 100 K. No perceptible MR nor MC were detected in BMO above the magnetic transition T_C. In the BFO films the resistance was too high to be resolved at all T investigated as mentioned before, and the MR could not be determined.

Figure 6(b) shows ε' vs f curves for BMO films collected under various applied H at 95 K. At low f, ε' shows an upturn, which represents the onset of the extrinsic Maxwell-Wagner relaxation R2-CPE2 [see $\varepsilon'_{\text{high}}$ in Fig. 2(a)], where perceptible variations with H occur. It has been pointed out in Sec. II. B that such variation in ε' with H in the vicinity of an extrinsic relaxation is not necessarily a reflection of MEC but can be caused entirely by the MR of an extrinsic Maxwell-Wagner relaxation.[40] Since the intrinsic BMO film relaxation shows perceptible MR, the extrinsic relaxation may be expected to exhibit similar behavior and the variation in ε' at low f observed in Fig. 6(b) may well be artificial and simply reflect the MR of the extrinsic Maxwell-Wagner relaxation. At higher f where the intrinsic relaxation is more dominant, only small MC can be seen. Intrinsic BMO ε_1 values were obtained from the circuit fits by extracting C1 for various H and the intrinsic MC, defined as MC=[C(H=0)–C(H)]/C(0), is shown in the inset of Fig. 6(b). Intrinsic MC and MEC appear to be rather small in the range of $\approx -1.5\%$ at 90 kOe, which confirms the rather weak peak feature in ε_1 vs T [Fig. 4(b)] and previous reports on polycrystals (MC$\approx -0.7\%$ at 90 kOe).[34] In the BFO films no MEC was detected, probably due to the fact that the antiferromagnetic transition temperature occurs at much higher T, and only near such transition, MC and MEC effects may be detectable.

VII. CONCLUSIONS

We have achieved deconvolution of intrinsic and extrinsic dielectric relaxations and the separation of MC and MR effects in BMO and BFO multiferroic epitaxial thin films by the analysis of f-, T-, and H-dependent impedance spectroscopy data using equivalent circuit-fitting procedures. A perceptible intrinsic MR effect of up to 65% was found in BMO films below T_C. MC as a result of intrinsic MEC near the BMO magnetic transition $T_C \approx 100$ K was identified unambiguously by a small peak feature in the ε_1 vs T curve, as well as by consistent trends of MC vs H at fixed T of 95 K and 100 K. Intrinsic MC and MEC in BMO films were found to be $\approx -1.5\%$ at 90 kOe, whereas BFO films showed no detectable MC in the T range investigated.

ACKNOWLEDGMENTS

The authors acknowledge financial support from the Spanish Ministerio de Ciencia e Innovación (MICINN) under Grants No. MAT2008-06761-C03, No. MAT2011-29269-C03, No. MAT2011-27470-C02, No. IMAGINE CSD2009-00013, No. CONSOLIDER INGENIO CSD2009-00013, Contract No. NANOSELECT CSD2007-00041, and from the Comunidad de Madrid through S2009-MAT1756 (PHAMA). R.S. and N.M.N. acknowledge the Ramón y Cajal program from the MICINN. Many thanks go to SSSS Ltd. for support with the data analysis.

*Corresponding author. rainerxschmidt@googlemail.com

[1]G. Lawes and G. J. P. D. A. P. Srinivasan, J. Phys. D **44**, 243001 (2011).
[2]N. A. Spaldin, S. W. Cheong, and R. Ramesh, Phys. Today **63**, 38 (2010).
[3]R. Ramesh, Nature (London) **461**, 1218 (2009).
[4]R. Ramesh and N. A. Spaldin, Nat. Mater. **6**, 21 (2007).
[5]M. Mostovoy, Nat. Mater. **9**, 188 (2010).
[6]J. Hemberger, P. Lunkenheimer, R. Fichtl, H. A. Krug von Nidda, V. Tsurkan, and A. Loidl, Nature (London) **434**, 364 (2005).
[7]J. Wu, J. Wang, D. Xiao, and J. Zhu, J. Appl. Phys. **110**, 064104 (2011).
[8]M. Fiebig, T. Lottermoser, D. Frohlich, A. V. Goltsev, and R. V. Pisarev, Nature (London) **419**, 818 (2002).
[9]J. Wang, J. Neaton, H. Zheng, V. Nagarajan, S. B. Ogale, B. Liu, D. Viehland, V. Vaithyanathan, D. G. Schlom, U. Waghmare, N. A. Spaldin, K. M. Rabe, M. Wuttig, and R. Ramesh, Science **299**, 1719 (2003).
[10]T. Kimura, G. Lawes, T. Goto, Y. Tokura, and A. P. Ramirez, Phys. Rev. B **71**, 224425 (2005).
[11]F. Yan, I. Sterianou, S. Miao, I. M. Reaney, M. O. Lai, and L. Lu, J. Appl. Phys. **105**, 074101 (2009).
[12]R. Martínez, A. Kumar, R. Palai, J. F. Scott, and R. S. Katiyar, J. Phys. D **44**, 105302 (2011).
[13]I. Fina, N. Dix, L. Fàbrega, F. Sanchez, and J. Fontcuberta, Thin Solid Films **518**, 4634 (2010).
[14]H. Zheng, J. Wang, S. E. Lofland, Z. Ma, L. Mohaddes-Ardabili, T. Zhao, L. Salamanca-Riba, S. R. Shinde, S. B. Ogale, F. Bai, D. Viehland, Y. Jia, D. G. Schlom, M. Wuttig, A. Roytburd, and R. Ramesh, Science **303**, 661 (2004).
[15]W. Eerenstein, M. Wiora, J. L. Prieto, J. F. Scott, and N. D. Mathur, Nat. Mater. **6**, 348 (2007).
[16]N. Ortega, A. Kumar, R. S. Katiyar, and C. Rinaldi, J. Mater. Sci. **44**, 5127 (2009).
[17]D. K. Pradhan, R. N. P. Choudhary, C. Rinaldi, and R. S. Katiyar, J. Appl. Phys. **106**, 024102 (2009).
[18]A. Srivastava, A. Garg, and F. D. Morrison, J. Appl. Phys. **105**, 054103 (2009).
[19]Y.-H. Chu, Q. Zhan, L. W. Martin, M. P. Cruz, P.-L. Yang, G. W. Pabst, F. Zavaliche, S.-Y. Yang, J.-X. Zhang, L.-Q. Chen, D. G. Schlom, I.-N. Lin, T.-B. Wu, and R. Ramesh, Adv. Mater. **18**, 2307 (2006).
[20]J. Wu and J. Wang, J. Am. Ceram. Soc. **93**, 2795 (2010).
[21]M. Azuma, H. Kanda, A. A. Belik, Y. Shimakawa, and M. Takano, J. Magn. Magn. Mater. **310**, 1177 (2007).
[22]S. Selbach, T. Tybell, M.-A. Einarsrud, and T. Grande, Chem. Mater. **21**, 5176 (2009).
[23]Y. Du, Z. X. Cheng, S. X. Dou, X. L. Wang, H. Y. Zhao, and H. Kimura, Appl. Phys. Lett. **97**, 122502 (2010).
[24]M. Gajek, M. Bibes, S. Fusil, K. Bouzehouane, J. Fontcuberta, A. Barthelemy, and A. Fert, Nat. Mater. **6**, 296 (2007).
[25]W. S. Choi, S. J. Moon, S. S. A. Seo, D. Lee, J. H. Lee, P. Murugavel, T. W. Noh, and Y. S. Lee, Phys. Rev. B **78**, 054440 (2008).
[26]D.-Y. Cho, J.-Y. Kim, B.-G. Park, K.-J. Rho, J.-H. Park, H.-J. Noh, B.-J. Kim, S.-J. Oh, H.-M. Park, J.-S. Ahn, H. Ishibashi, S.-W. Cheong, J. H. Lee, P. Murugavel, T. W. Noh, A. Tanaka, and T. Jo, Phys. Rev. Lett. **98**, 217601 (2007).
[27]R. Kajimoto, H. Sagayama, K. Sasai, T. Fukuda, S. Tsutsui, T. Arima, K. Hirota, Y. Mitsui, H. Yoshizawa, A. Q. R. Baron, Y. Yamasaki, and Y. Tokura, Phys. Rev. Lett. **102**, 247602 (2009).
[28]F. Zavaliche, H. Zheng, L. Mohaddes-Ardabili, S. Y. Yang, Q. Zhan, P. Shafer, E. Reilly, R. Chopdekar, Y. Jia, P. Wright, D. G. Schlom, Y. Suzuki, and R. Ramesh, Nano Lett. **5**, 1793 (2005).
[29]See Supplemental Material at http://link.aps.org/supplemental/10.1103/PhysRevB.86.035113 for detailed descriptions on I. Simulations of dielectric spectroscopy data. II. BMO and BFO thin-film deposition. III. XRD of thin films. IV. AFM. V. PFM. VI. Magnetic film characterization. VII. Alternative representations of dielectric spectroscopy data.
[30]T. Kimura, T. Goto, H. Shintani, K. Ishizaka, T. Arima, and Y. Tokura, Nature (London) **426**, 55 (2003).
[31]T. Goto, T. Kimura, G. Lawes, A. P. Ramirez, and Y. Tokura, Phys. Rev. Lett. **92**, 257201 (2004).
[32]J. Hemberger, F. Schrettle, A. Pimenov, P. Lunkenheimer, V. Y. Ivanov, A. A. Mukhin, A. M. Balbashov, and A. Loidl, Phys. Rev. B **75**, 035118 (2007).
[33]T. Katsufuji, S. Mori, M. Masaki, Y. Moritomo, N. Yamamoto, and H. Takagi, Phys. Rev. B **64**, 104419 (2001).
[34]T. Kimura, S. Kawamoto, I. Yamada, M. Azuma, M. Takano, and Y. Tokura, Phys. Rev. B **67**, 180401(R) (2003).
[35]B. Lorenz, Y. Q. Wang, Y. Y. Sun, and C. W. Chu, Phys. Rev. B **70**, 212412 (2004).
[36]F. Schrettle, P. Lunkenheimer, J. Hemberger, V. Y. Ivanov, A. A. Mukhin, A. M. Balbashov, and A. Loidl, Phys. Rev. Lett. **102**, 207208 (2009).
[37]T. Suzuki and T. Katsufuji, Phys. Rev. B **77**, 220402(R) (2008).
[38]W. Wang, L. Zhang, D. Yuan, and Y. Sun, Thin Solid Films **518**, 7044 (2010).
[39]Y. Yamasaki, S. Miyasaka, T. Goto, H. Sagayama, T. Arima, and Y. Tokura, Phys. Rev. B **76**, 184418 (2007).
[40]G. Catalan, Appl. Phys. Lett. **88**, 102902 (2006).
[41]J. T. S. Irvine, D. C. Sinclair, and A. R. West, Adv. Mater. **2**, 132 (1990).
[42]E. Barsukov and J. Macdonald, *Impedance Spectroscopy: Theory, Experiment and Applications* (Wiley, Hoboken, NJ, 2005).
[43]R. Schmidt, W. Eerenstein, T. Winiecki, F. D. Morrison, and P. A. Midgley, Phys. Rev. B **75**, 245111 (2007).
[44]E. J. Abram, D. C. Sinclair, and A. R. West, J. Electroceram. **10**, 165 (2003).
[45]P. Lunkenheimer, R. Fichtl, S. G. Ebbinghaus, and A. Loidl, Phys. Rev. B **70**, 172102 (2004).
[46]C. H. Hsu and F. Mansfeld, Corrosion **57**, 747 (2001).
[47]W. Eerenstein, F. D. Morrison, J. Dho, M. G. Blamire, J. F. Scott, and N. D. Mathur, Science **307**, 1203a (2005).
[48]W. Eerenstein, F. D. Morrison, J. F. Scott, and N. D. Mathur, Appl. Phys. Lett. **87**, 101906 (2005).
[49]R. Schmidt, W. Eerenstein, and P. A. Midgley, Phys. Rev. B **79**, 214107 (2009).
[50]A. K. Jonscher, J. Phys. D **32**, R57 (1999).
[51]A. Isnin and A. K. Jonscher, Ferroelectrics **210**, 47 (1998).
[52]T. Nattermann, Y. Shapir, and I. Vilfan, Phys. Rev. B **42**, 8577 (1990).

[53]D. Damjanovic, Phys. Rev. B **55**, R649 (1997).
[54]W. Kleemann, Annu. Rev. Mater. Res. **37**, 415 (2007).
[55]A. K. Jonscher, *Dielectric Relaxation in Solids* (Chelsea Dielectrics, London, 1983).
[56]H. Naohiro, PhD Thesis, University of Aberdeen, 1995.
[57]R. Schmidt and A. W. Brinkman, J. Appl. Phys. **103**, 113710 (2008).
[58]B. I. Shklovskii and A. L. Efros, *Electronic Properties of Doped Semiconductors* (Springer-Verlag, Berlin, 1984).
[59]R. Schmidt, A. Basu, and A. W. Brinkman, Phys. Rev. B **72**, 115101 (2005).
[60]J. M. D. Coey, M. Viret, L. Ranno, and K. Ounadjela, Phys. Rev. Lett. **75**, 3910 (1995).
[61]R. Schmidt, Phys. Rev. B **77**, 205101 (2008).